POSCA: Path Optimization for Solar Cover Amelioration in Urban Air Mobility

Debjyoti Sengupta, Anurag Satpathy, and Sajal K. Das
Department of Computer Science
Missouri University of Science and Technology, Rolla, USA
E-mail: {dsengupta, anurag.satpathy, sdas}@mst.edu

2024 IEEE International Conference on Smart Computing (SMARTCOMP) | 979-8-3503-4994-8/24/$31.00 ©2024 IEEE | DOI: 10.1109/SMARTCOMP61445.2024.00023

***Abstract*—Urban Air Mobility (UAM) encompasses both piloted and autonomous aerial vehicles, spanning from small unmanned aerial vehicles (UAVs) like drones to passenger-carrying personal air vehicles (PAVs), to revolutionize smart transportation in congested urban areas. This emerging paradigm is anticipated to offer disruptive solutions to the mobility challenges in congested cities. In this context, a pivotal concern centers on the sustainability of transitioning to this mode of transportation, especially with the focus on incorporating clean technology into developing innovative solutions from the ground up. Recent studies highlight that a significant portion of the total energy consumption in UAM can be attributed to the flight operations of the aircraft. To address this challenge, this paper introduces a framework POSCA aimed at meeting the energy requirements of UAM flights. It delves into a complex and dynamic route-planning problem. It introduces a novel concept called the Phototropic Index, calculated by considering the traversal distance and solar coverage along the route. To solve the path planning problem, we propose two solutions, S-POSCA and D-POSCA, catering to static and dynamic setups. Simulation results confirm an average increase of 8.81% in static conditions and 10.64% in the dynamic condition for the cumulative Global Horizontal Irradiance (GHI) compared to the baseline approaches.**

***Index Terms*—Urban air mobility, vertical take-off and landing vehicles, dynamic route-planning, path optimization, solar energy.**

I. Introduction

With rapid urbanization and migration of a large fraction of rural populations to major cities, some new and unique fundamental computational challenges have emerged. Some of them include developing stable, manageable, safe, and efficient transportation networks. Due to urban sprawl, the existing transportation capabilities of a city can become saturated, proving insufficient for supporting the increased mobility needs [1]. Major cities experience unusually large average travel times due to traffic. New York City experienced an average travel time of $(24min\ 50s)/10km$ while London had the worst traffic in the world requiring $(37min\ 20s)/10km$ trip in 2023 [2]. Thus, to enhance the capacity of existing transportation networks while providing feasible economic and reliable solutions, alternative transport modes are needed.

Urban Air Mobility (UAM) is envisioned to encompass various categories of vehicles designed for specific purposes. These vehicles may range from small unmanned aerial vehicles (UAVs), such as drones, to passenger-carrying vehicles having higher payload capacity and robust autonomous capabilities [1]. In the current aviation industry, flight schedules, routes, and demands are well-defined, and various commercial aircraft are designed and allocated accordingly. However, the UAM market is expected to be dominated by 'on-demand' flights (Fig. 1), resulting in frequently changing flight demands for flight routes, making vertical take-off and landing (VTOL) vehicles are the primary contenders for UAM.

Fig. 1. An instance of an On Demand UAM flight reducing travel time to 15 minutes instead of 50 minutes in a congested road network.

There has been a recent surge in the research and development of electric VTOL (eVTOL) vehicles with the UAM market getting closer to realization owing to the advancement of distributed propulsion technology. Examples include the ALIA-250, an aircraft jointly developed by Blade and Beta [3], which conducted its first test flight in February 2023 in New York City and Alef Aeronautics is a SpaceX-backed startup based in San Mateo, California. Alef Aeronautics recently unveiled their flying car concept, capable of running on the road as a normal car while transitioning into sustained flight as an eVTOL [4]. The UAM market is expected to be dominated by piloted aircraft initially, followed by remotely operated aircraft with a one-to-one correspondence between the pilot and vehicle. This pilot-to-vehicle ratio is expected to decrease over time, paving the way for fully autonomous vehicles.

The UAM market is projected to grow from US $3 billion in 2021 to US $8.91 billion in 2028 [5]. Since UAM is expected to occupy a large share of the transportation market by volume, efforts need to be made to reduce the ecological footprint of this new technology by adopting sustainable, eco-friendly

2693-8340/24/$31.00 ©2024 IEEE
DOI 10.1109/SMARTCOMP61445.2024.00023

practices right from its inception. The sustainability of this new transportation paradigm has been studied to a considerable extent in [6], [7]. The analysis done in [8] reveals that most of the energy is consumed during the flight of UAM aircraft as opposed to ground operations, posing a big challenge to the sustainability of its operation. Also, efficient path planning of UAM vehicles from source to destination depends on weather and traffic conditions in the airspace, which are often dynamic.

Though nearing commercialization, UAM is still at the planning stage thereby, no concrete regulation as to the structure and management of the UAM airspace is available. Some preliminary work in planning 3D airspace [9] and estimation of demand for UAM [10] provide valuable insights. At the outset, the path planning problem appears to be facile; however, there are some intrinsic challenges. To elaborate, the problem undertaken in this paper encompasses ameliorating the solar cover during the trip, keeping the deviation from the shortest path to a minimum to meet traversal time constraints. This is a variant of the Multi-Objective Shortest Path (MOSP) problem, proven to be $\mathcal{NP}$-Hard [11].

Our Contributions: Motivated by the above research challenges and limitations of the existing literature, we in this paper address the sustainability aspect of UAM, presenting a novel framework POSCA[§] with the following contributions.

- We propose a sustainable method of charging UAM vehicles by integrating the harnessing of solar energy in the path planning stage itself.
- We introduce a novel *Phototropic Index* to characterize the charging capacity of a sector and the tendency of a UAM vehicle to fly towards it in the airspace, which draws inspiration from the natural phenomenon of phototropism observed in plants.
- Based on the Phototropic Index of sectors, we solve a dynamic route planning problem for finding the optimal path from source to destination such that solar energy is harvested to the maximum extent possible while meeting the traversal time constraint of the aerial vehicle.
- We convert MOSP to a Single-Objective Shortest Path (SOSP) problem by incorporating the Phototropic Index as a heuristic modification of the edge weights in the modified airspace graph. The resulting SOSP is solved using two different strategies: S-POSCA (*static variant*) and D-POSCA (*dynamic variant*). Through exhaustive simulations, we observe an average increase of 8.81% in static condition and 10.64% in the dynamic condition in the cumulative Global Horizontal Irradiance (GHI).

The paper is structured as follows: Section II reviews related work, while Section III outlines the system model and problem formulation. Section IV elaborates on the adopted solution approach. Results are analyzed in Section V, with a sample case study provided in Section VI. The features and limitations of POSCA are discussed in Section VII. Finally, Section VIII offers concluding remarks.

[§]Posca: an ancient roman energy drink commonly used by the soldiers on the battlefield.

II. Related Work

There has been some general work related to the design and development of UAM vehicles, and it also focuses on harnessing solar energy, which is discussed here.

A. The Case for Solar Energy

UAM is expected to rely heavily on eVTOL vehicles, as it offers a renewable energy-based solution that reduces the ecological footprint. Even though charging stations are the conventional means of replenishing the exhausted electrical energy of electric power-train-equipped vehicles, it translates to the vehicles being grounded for a considerable time to get recharged. This might mean financial loss for the organization operating these vehicles in the form of missed customer trips or the deployment of more aircraft to cater to the same amount of passengers. Using solar energy for charging allows harnessing a clean and freely available energy source. It allows the charging of such crafts without being physically plugged into a conventional charging station, paving the way for charging the vehicle during traversal [12].

For autonomous aerial vehicles especially, solar energy can be of greater significance as it allows the vehicle to charge via solar panels, which does away with the need to plug in, thereby removing the necessity of human intervention for charging. This leads to indefinitely extending the presence and mission duration [13]. In [13], this concept was used to develop an aircraft capable of charging itself off of solar energy while hibernating on the ground. This allowed the vehicle to carry out its operations again the next day after being fully charged by the Sun, thereby increasing the duration of the autonomous mission. Even though it is very useful in some scenarios that require repetition of similar flight behavior in a given area, it is not suitable for carrying passengers in the scope of UAM because: (*i*) the route or area of coverage of the vehicle is not fixed, as UAM is characterized by *on demand* nature of flights, (*ii*) it might not always be feasible to enter into a state of hibernation on the ground in between or even during flights.

B. Challenges Specific to UAM

There is a need to develop solutions that reduce the time the vehicle spends on the ground for charging. This requirement has given birth to the sub-field of perpetual-flight solar-powered fixed-wing aircraft, typically defined as High-Altitude Long-Endurance (HALE) [14], [15]. In this design ideology, the aircraft are characterized by the need to remain in the air for long periods, even extending to transoceanic flights. Therefore, these aerial vehicles are usually equipped with large wing aspect ratios to accommodate a large array of solar cells to achieve feasible charging capability and generate enough aerodynamic lift, thereby harnessing the advantages of conventional fixed-wing aircraft.

However, this design ideology cannot be applied to UAM because of the following reasons: (1) UAM is not expected to cover transoceanic flights and so the flight duration does need to be as long as in HALE; (2) UAM needs smaller, agile aircraft capable of ferrying passengers from congested

road networks via a designated, comparatively low-altitude airspace: and (3) HALE aircraft require much larger and stronger air-frames that are not required for UAM air taxis, which are required to be moderately sized for carrying passengers on comparatively shorter trips and also be economically feasible and accessible to a much larger population.

C. Research Gap in Existing Work

In [14], the focus is on designing an aircraft capable of achieving maximum input-to-output power ratio so that maximum energy efficiency can be obtained, given enough sunlight. But this assumes that there is enough sunlight during the charging period of the craft.

Most of the work done in this area till now has been aimed at the vehicle design aspect, as in [16]. However, the utility of such aircraft can be increased by looking into computational aspects which may be able to guide them or even smaller ones having less efficient solar charging capacities through a path that provides maximum sunlight while passing through areas with varying weather conditions.

A step in this direction is exhibited in [17], where the altitude of a solar-powered aircraft is varied to minimize the energy losses during flight and enable travel along the fastest possible way from source to destination without utilizing battery power provided the solar energy available is sufficient for the flight. So, this dealt with optimizing energy loss by controlling the altitude. In contrast, this paper aims to optimize the flight route to facilitate maximal charging *en route* while meeting the flight's arrival time deadline.

III. System Model and Problem Formulation

This section describes the airspace model and phototropic index computation, and formulate the problem.

A. Airspace Model

The airspace model, as shown in Fig. 2, can be envisioned as a homogeneous and contiguous set of sectors captured in the set $\mathcal{S} = \{s_1, s_2, ..., s_n\}$ [18], where $s_i \in \mathcal{S}$ uniquely identifies the sector 'i'. Note that the airspace can be transformed into a weighted undirected graph $\mathcal{G}^{\mathcal{A}} = (\mathcal{V}^{\mathcal{A}}, \mathcal{E}^{\mathcal{A}})$, wherein $\mathcal{V}^{\mathcal{A}}$ is the set of vertices corresponding to the centroids of the sectors and $\mathcal{E}^{\mathcal{A}}$ captures the edges connecting the adjacent sectors. For a sector $s_i \in \mathcal{S}$, the subset $\mathcal{N}(s_i) \subset \mathcal{S}$ represents the neighbors of s_i. A route from s_i to any of its neighbour $s_j \in \mathcal{N}(s_i)$ is captured via an edge $e_{i,j}$, such that $e_{i,j} \in \mathcal{E}^{\mathcal{A}}$.

UAM Flight Parameters: An UAM flight trip is represented by the tuple $< s_o, s_d, \tau, v >$ where s_o represents the origin sector of the flight; s_d represents the destination sector; τ represents the traversal time limit, i.e., the time by which the flight is to reach sector s_d; and v is taken to be a constant velocity at which the VTOL travels through the route

Note that v is considered constant throughout the flight trip for this work. To the best of our knowledge, no traffic flow model exists specifically designed for UAM.

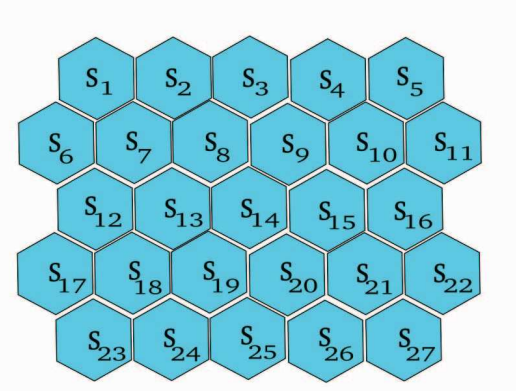

Fig. 2. Illustration of a Sample Airspace with 27 identical hexagonal sectors.

B. Phototropic Index

We propose using a potential energy surface [19] over the UAM airspace to find points with the lowest potential, which cause the path of aerial vehicles to be naturally directed towards them. Consequently, we construct the potential function so that the destination point (or sector in our scenario) has the lowest global potential, favorably zero. Accordingly, a potential function is proposed based on the normalized Euclidean Distance $\overline{r}(s_i, s_d)$ of the sector s_i to the destination sector s_d and the amount of sunlight measured in terms of Global Horizontal Irradiance (GHI) of a sector. To combine it with $\overline{r}(s_i, s_d)$, we use the normalized GHI denoted by $\overline{G}(s_i)$. This potential function is termed as the "*Phototropic Index*" of the sector and is computed as per Eq. (1).

$$\Pi(s_i) = k \cdot \frac{\overline{r}(s_i, s_d)}{\overline{G}(s_i)}; \ \ \forall\, i, d \in [1, n] \tag{1}$$

where k is a proportional constant (in m). It is to be noted that a sector closer to the destination will have lower potential, thereby *attracting* the trajectory of vehicles towards itself, acting as a global minimum of the airspace having $\Pi(s_i) = 0$. A sector with greater GHI value attracts the UAM vehicle towards itself, exhibiting positive phototropism.

However, if the airspace is being traversed by multiple aerial vehicles at a time, which presents a more practical scenario, such a definition of the Phototropic Index would mean that every vehicle selects the same flight path to the destination provided they are using the same algorithm for path selection. In reality, there is a limit to the number of aircraft that can be accommodated, rather than allowed to safely occupy a given sector s_i at any point in time, referred to as the *sector capacity*, denoted by $\mathcal{C}(s_i)$. A sector occupied by several aircraft $\mathcal{P}(s_i)$ equal to its capacity can be treated as *blocked* to find the flight path. In other words, the cost to travel to this sector should be ∞. To incorporate this into the expression of $\Pi(s_i)$, we modify Eq. (1) and obtain Eq. (2).

$$\Pi(s_i) = k \cdot \frac{\overline{r}(s_i, s_d)}{\mathcal{I}(s_i) \cdot \overline{G}(s_i)}; \ \ \forall\, i, d \in [1, n] \tag{2}$$

where,

$$\mathcal{I}(s_i) = \begin{cases} 0, & \text{If} \quad \mathcal{C}(s_i) - \mathcal{P}(s_i) = 0 \\ 1, & \text{Otherwise} \end{cases}$$

Here $\mathcal{I}(s_i)$ is an indicator variable which equals 0 when a sector is filled, making $\Pi(s_i) = \infty$ and distributing the entire traffic over various routes by putting a cap on the number of aircraft allowed in a sector at any given time. This sector capacity is usually set and enforced by the administrative body governing airspace operations.

Now we map the Phototropic Index of the sectors as mentioned in Eq. (2) to the cost of traveling between two sectors, which are nothing but the edge weights in the graph of the airspace $\mathcal{G}^{\mathcal{A}}(\mathcal{V}^{\mathcal{A}}, \mathcal{E}^{\mathcal{A}})$, where $e_{i,j} = (s_i, s_j) \in \mathcal{E}^{\mathcal{A}}$.

Based on the condition for edge costs in D* Lite Algorithm [20], the edge cost to transit from s_i to s_j is in the range $0 < c(s_i, s_j) \leq \infty$. The edge costs of an edge connecting s_i to s_j in the modified graph $\mathcal{G}'^{\mathcal{A}}$ is derived as per Eq. (3).

$$c(s_i, s_j) = r(s_i, s_j) + \Pi(s_j) \tag{3}$$

C. Problem Formulation

A path from origin s_o to destination s_d is a sequence of sectors given by $\boldsymbol{P} = < s_o, s_1, s_2, \ldots, s_i, s_{i+1}, s_d >$, where (s_i, s_{i+1}) is an edge $e_{i,j} \in \mathcal{E}^{\mathcal{A}}$. The overall problem is captured in Eq. (4a), the traversal time constraint in Eq. (4b), and the feasible range of decision variables in Eqs. (4c)-(4f).

$$minimize \sum_{e_{i,j} \in P} c(s_i, s_j) \tag{4a}$$

$$s.t. \quad \frac{\sum_{e_{i,j} \in P} r(s_i, s_j)}{v} \leq \tau \tag{4b}$$

$$\mathcal{I}(s_i) \in \{0, 1\} \tag{4c}$$

$$0 < c(s_i, s_j) \leq \infty \tag{4d}$$

$$0 \leq \mathcal{P}(s_i) \leq \mathcal{C}(s_i) \tag{4e}$$

$$\forall\, i, j \in [1, n] \tag{4f}$$

The MOSP problem is proven to be $\mathcal{NP}$-Hard [11]. The problem is transformed into SOSP via the Phototropic Index captured by edge weights in $\mathcal{G}'^{\mathcal{A}}$. This effectively captures the bi-objective problem of the shortest path while improving the solar cover, facilitating a polynomial time solution.

IV. Proposed Solution Approach

Since we modeled the airspace as hexagonal sectors identical in size and shape [18] [21], we first view the considered airspace as a graph as illustrated in Fig. 3. The centroid of each sector is taken to be the position of the corresponding vertex, and the physical distance between any two sectors is the distance between their respective centroids.

The scope of this work is divided into two major parts: *static*, where the condition of the sectors is considered to be constant in terms of GHI values and traffic condition (occupancy of a sector by vehicles at an instant) and *dynamic*, which resembles a more practical scenario where the weather and traffic conditions can change while the aircraft is in transit.

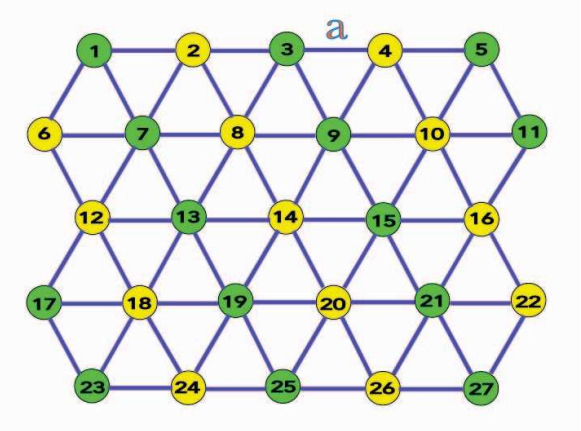

Fig. 3. Graph constructed for chosen airspace: each vertex represents a sector, and only adjacent sectors are connected by an edge. The distance between any adjacent sectors is a constant (denoted by a).

A. Static-POSCA (S-POSCA)

The overall execution of S-POSCA follows Algorithm 1. The airspace graph ($\mathcal{G}^{\mathcal{A}}$), source ($s_o$) and destination ($s_d$) sector, and the capacity ($\mathcal{C}(s_i)$), population ($\mathcal{P}(s_i)$) and coordinates ((x_i, y_i)) of each sector are taken as inputs to the algorithm. The algorithm outputs the shortest path from the source to the destination in $\boldsymbol{P}$. The algorithm is initiated by computing the Phototropic Index and subsequently updating the edge weights in an updated graph ($\mathcal{G}'^{\mathcal{A}}$) (Steps 2-3). Next, Dijkstra's Algorithm is executed on the updated graph and the path from s_o to s_d is returned as output. Note that we use the regular *Dijkstra's Algorithm* to obtain the shortest path [22]. Algorithm 1 can be executed for two cases: with traffic congestion (as per Eq. (2)), and without the traffic consideration (as per Eq. (1)).

Algorithm 1: S-POSCA

Input: $\mathcal{G}^{\mathcal{A}}$, s_o, s_d, $G(s_i)$, $\mathcal{C}(s_i)$, $\mathcal{P}(s_i)$, (x_i, y_i) $\forall$ $s_i \in \mathcal{S}$
Result: $\boldsymbol{P}$ ▷ Shortest Path
1 **Initialize**: $\Pi(s_i) = \Phi$, $\forall$ $s_i \in \mathcal{S}$; $\boldsymbol{P} = \Phi$
2 Calculate $\Pi(s_i)$ $\forall$ $s_i \in \mathcal{S}$ as per Eq. (1) or (2)
3 Update edge costs $c(s_i, s_j)$ as per Eq. (3) $\forall$ $e_{i,j} \in \mathcal{E}^{\mathcal{A}}$ to get updated graph $\mathcal{G}'^{\mathcal{A}}$
4 $\boldsymbol{P}$ = **Dijkstra**($\mathcal{G}'^{\mathcal{A}}, s_o, s_d$) ▷ Regular Dijkstra
5 return $\boldsymbol{P}$

B. Dynamic-POSCA (D-POSCA)

For the dynamic condition, we employ the *D* Lite Algorithm* [20], owing to its efficiency in identifying modified edge weights and updating only the ones that matter when calculating the path from source to destination. The overall working of D-POSCA is captured in Algorithm 2. The inputs to the algorithm include the the airspace graph ($\mathcal{G}^{\mathcal{A}}$), source ($s_o$) and destination ($s_d$) sector, and the capacity ($\mathcal{C}(s_i)$), population ($\mathcal{P}(s_i)$) and coordinates ((x_i, y_i)) of each sector. The algorithm outputs the shortest path from the source to the destination in $\boldsymbol{P}_{s_c}$. The algorithm is initiated by computing the Phototropic Index and subsequently updating the edge weights in an updated graph ($\mathcal{G}'^{\mathcal{A}}$) (Steps 2-3). Next, D* Lite

executes on the updated graph, and an initial path from s_o to s_d is obtained and retained in P_{s_o}. As per P_{s_c} (same as P_{s_o} initially), the traversal of the UAM vehicle starts. On reaching the current sector (s_c), the next sector to be visited is checked using **Peep**(.), retained in s_c using **Pop**(.), and appended to the list $\boldsymbol{P}_T$ using **Append**(.). In the next step, the algorithm gets the updated GHI values and consequently recomputes $\Pi(s_i)$ for un-traversed sectors. As per the updated $\Pi(s_i)$ values, D* Lite is again invoked and executed from **Peep**($\boldsymbol{P}_{s_c}$) to s_d. Depending on the total traversal time either of the cases are encountered: (*i*.) the traversal time requirement (τ) is satisfied, (*ii*.) not satisfied. In the former, the algorithm continues execution with an updated $\boldsymbol{P}_{s_c}$, whereas in the latter the algorithm terminates with the current path (Steps 6-14).

Algorithm 2: D-POSCA

Input: $\mathcal{G}^{\mathcal{A}}$, s_o, s_d, $G(s_i)$, $\mathcal{C}(s_i)$, $\mathcal{P}(s_i)$, (x_i, y_i),$\forall\ s_i \in \mathcal{S}$
Result: $\boldsymbol{P}_{s_c}$ ▷ Shortest Path
1 **Initialize**: $\Pi(s_i) = \Phi$, $\forall\ s_i \in \mathcal{S}$; $\boldsymbol{P}_{s_c} = \Phi, \boldsymbol{P}_T = \Phi, s_c = s_o$
2 Calculate $\Pi(s_i)$, $\forall\ s_i \in \mathcal{S}$ as per Eq. (2)
3 Update edge costs $c(s_i, s_j)$ as per Eq. (3), $\forall\ e_{i,j} \in \mathcal{E}^{\mathcal{A}}$ to get updated graph $\mathcal{G}'^{\mathcal{A}}$
4 $\boldsymbol{P}_{s_o}$ = **D* Lite**($\mathcal{G}'^{\mathcal{A}}, s_o, s_d$) ▷ D* Lite
5 $\boldsymbol{P}_{s_c} = \boldsymbol{P}_{s_o}$;
6 **while** (***Peep***($\boldsymbol{P}_{s_c}$) $\neq s_d$) **do**
7 s_c = **Pop**($\boldsymbol{P}_{s_c}$) ▷ When vehicle at s_c
8 $\boldsymbol{P}_T$ = **Append**($\boldsymbol{P}_T, s_c$) ▷ Add s_c to traversed path
9 Get updated values of $G(s_i)$, $\forall s_i \in \mathcal{S}$
10 Re-calculate $\Pi(s_i)$, $\forall\ s_i \in \mathcal{S}$ as per Eq. (2)
11 $\boldsymbol{P'}_{s_c}$ = **D* Lite**($\mathcal{G}'^{\mathcal{A}}$, **Peep**($\boldsymbol{P}_{s_c}$), s_d)
12 **if** $\frac{(|\boldsymbol{P}_T| + |\boldsymbol{P'}_{s_c}|) \times a}{v} > \tau$ **then**
13 return $\boldsymbol{P}_{s_c}$
14 $\boldsymbol{P}_{s_c} = \boldsymbol{P'}_{s_c}$

Theorem 1. *The Phototropic Index $\Pi(s_i)$ ensures that the cost of travel to a sector s_i is always less than that to sector $s_{i'}$ ($i \neq i'$) where $G(s_i) > G(s_{i'})$ provided all other properties are equal between the two.*

Proof: We consider the current node (or sector) to be s_0, from which we have two best possible options s_i and $s_{i'}$, both equidistant from s_0. We consider that s_i and $s_{i'}$ are equidistant from the goal vertex (or sector). Also $\mathcal{C}(s_i) = \mathcal{C}(s_{i'})$ and $\mathcal{P}(s_i) = \mathcal{P}(s_{i'})$, and $G(s_i) > G(s_{i'})$. Thus $\Pi(s_i) < \Pi(s_{i'})$. As per Eq. (3):

$$c(s_0, s_i) = r(s_0, s_i) + \Pi(s_i) \quad and$$
$$c(s_0, s_{i'}) = r(s_0, s_{i'}) + \Pi(s_{i'}).$$

Subtracting the second expression from the first, we get,

$$c(s_0, s_i) - c(s_0, s_{i'}) = \Pi(s_i) - \Pi(s_{i'})$$
$$[as \quad r(s_0, s_i) = r(s_0, s_{i'})].$$

$$\therefore \ \ c(s_0, s_i) < c(s_0, s_{i'})$$

Hence, the cost of travel to s_i is less than that to $s_{i'}$ when $G(s_i) > G(s_{i'})$, and all other sector properties are equal. ■

Theorem 2. ***(Time Complexity)**: S-POSCA has an asymptotic complexity of $O(|\mathcal{V}^{\mathcal{A}}| \log |\mathcal{V}^{\mathcal{A}}|)$, which is polynomial.*

Proof: S-POSCA first calculates the Phototropic Index $\Pi(s_i)$ for all sectors in $O(|\mathcal{V}^{\mathcal{A}}|)$. Next, Dijkstra's Algorithm executes on the modified graph $\mathcal{G}'^{\mathcal{A}}$ in $O((|\mathcal{V}^{\mathcal{A}}| + |\mathcal{E}^{\mathcal{A}}|) \log |\mathcal{V}^{\mathcal{A}}|)$ as adjacency list is used for graph representation. Since $\mathcal{G}'^{\mathcal{A}}$ has a maximum degree of 6, $|\mathcal{E}^{\mathcal{A}}| \approx 6|\mathcal{V}^{\mathcal{A}}|$, making the overall time complexity of Dijkstra's $O(|\mathcal{V}^{\mathcal{A}}| \log |\mathcal{V}^{\mathcal{A}}|)$. So the total complexity is $O(|\mathcal{V}^{\mathcal{A}}|) + O(|\mathcal{V}^{\mathcal{A}}| \log |\mathcal{V}^{\mathcal{A}}|) = O(|\mathcal{V}^{\mathcal{A}}| \log |\mathcal{V}^{\mathcal{A}}|)$. ■

Theorem 3. ***(Time Complexity)**: D-POSCA has an asymptotic complexity of $O(6^{\sqrt{|\mathcal{V}^{\mathcal{A}}|}})$.*

Proof: D-POSCA relies on the D* Lite algorithm to calculate the shortest path to the destination after each successive sector hop of the UAM vehicle. After each sector hop, the $\Pi(s_i)$ values are updated for all sectors in $O(|\mathcal{V}^{\mathcal{A}}|)$ time. Now, since the D* Lite is selected based on its efficiency to compute only upon the nodes affected by modified edge weights in the graph that are significant in calculating the shortest path to destination s_d, there is no fixed time complexity of the algorithm. It depends on the extent of the dynamic changes in edge weights of $\mathcal{G}'^{\mathcal{A}}$ and the efficiency of the heuristic used. Considering the worst-case scenario where all of the edge weights change due to changes in respective $G(s_i)$ values, the time complexity of D* Lite approaches the order of $O(b^d)$ as in the case of a standard uninformed search like Depth-First-Search (DFS). However, due to the nature of $\mathcal{G}^{\mathcal{A}}$, the branching factor b is limited to 6 (maximum degree of a sector) and d is the path length, which in the worst case would involve traversing $\mathcal{G}'^{\mathcal{A}}$ along the boundary nodes, from a corner to another corner of the airspace. So given an airspace having $\mathcal{V}^{\mathcal{A}}$ sectors, the longest path would be of $O(\sqrt{|\mathcal{V}^{\mathcal{A}}|})$, thereby limiting the complexity of D-POSCA to $O(6^{\sqrt{|\mathcal{V}^{\mathcal{A}}|}})$. ■

V. Performance Evaluation

The components of the experimental setup are discussed, along with the dataset used for mimicking real-world GHI values, and the results obtained are presented.

A. Experimental Setup

Fig. 2 shows the airspace under consideration for experimentation. A node represents each of the sectors, and the resulting graph in Fig. 3 is used as the input to the algorithm. To demonstrate the advantage of using the Phototropic Index to increase solar cover, the same set of origin and destination sectors are used for calculating the shortest paths based on a conventional graph, where the edge weights are the physical distances between sectors (2 km in our setup) and on a modified version of the same graph having the same topology but updated edge weights as per Eq. (3). For closer inspection of the variation in path due to consideration of just the solar cover vs that of both solar cover and traffic congestion, we use both expressions of $\Pi(s_i)$ as given by equations (1) and (2) to update the edge costs. Deviation in flight path from the shortest path (obtained from Dijkstra's Algorithm) is shown for both cases in Fig. 4 and 5 for an instance where the origin sector is s_{18} and s_{11} the destination.

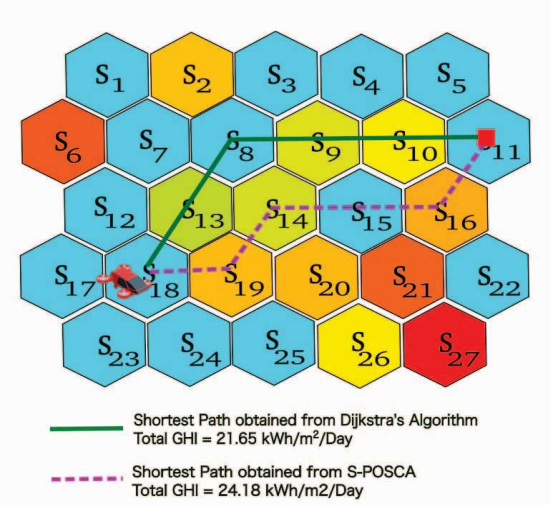

Fig. 4. Shortest Path without and with S-POSCA. Pale yellow sectors have less GHI, orange ones have greater values, and dark red ones have the maximum. Blue sectors represent insignificant GHI values.

B. NSRDB Dataset

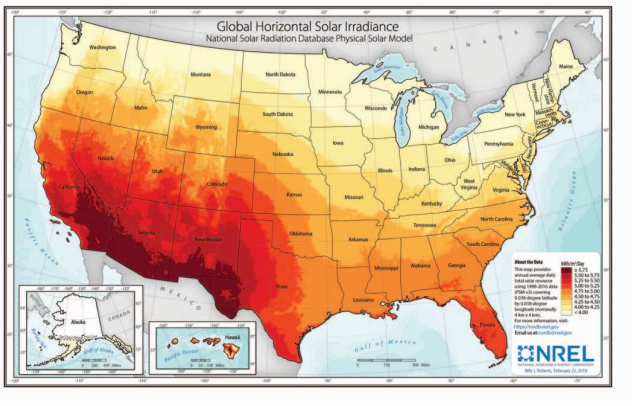

Fig. 6. Global Horizontal Irradiance NSRDB Map.

The GHI values for each of the sectors in the chosen airspace for experimental analysis are based on real-world observations extracted from the National Solar Radiation Database (NSRDB) dataset [23], [24]. This database is maintained by the National Renewable Energy Laboratory (NREL) and has the Global Horizontal Irradiance (GHI) values of various regions worldwide. Each region is approximately of the dimension $4km \times 4km$. The map in Fig. 6 provides the daily mean GHI value of a certain region all over the USA in $kWh/m^2/Day$, which is the conventional unit to denote the amount of solar energy available based on GHI.

For our experimental purpose, however, we use the most recent data of the year 2022 for a small area in Missouri, encompassing the cities of Rolla and St. James. The database has the GHI values of various locations in the said area recorded at every 30-minute interval, thereby providing us with a realistic dataset for the simulation of a flight in UAM. In this work, the average GHI values at every 30-minute mark over a randomly chosen set of specific locations within said area were considered. Careful observation shows that

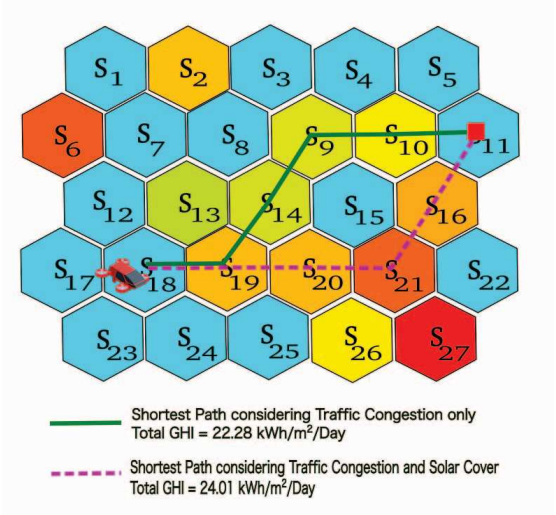

Fig. 5. Shortest Path *considering* traffic Congestion without and with S-POSCA.

TABLE I
CONVERSION TABLE FOR GHI UNITS.

Input Unit	Conversion Factor	Output Unit
W/m^2	0.024	$kWh/m^2/Day$
$kWh/m^2/Day$	41.666	W/m^2

the most GHI values recorded (around 80%) lie in the (50-600) W/m^2 range, which translates to a range of (1.2-19.2) $kWh/m^2/Day$ (conversion factor mentioned in Table I).

Global Horizontal Irradiance (GHI) denotes the total amount of incoming solar radiation received by a surface horizontal to the ground. It is the sum of *Direct Normal Irradiance* (DNI) and *Diffuse Horizontal Irradiance* (DIF). Since a solar-charging capable aircraft is expected to fly through the airspace by exhibiting a variety of maneuvers necessary for stable flight, there is no guarantee that the photovoltaic surfaces on the aerial vehicle will always face the sun directly. So, the GHI values are considered to account for the entire amount of solar radiation incident, both directly and through diffusion. For the experiment, we use the range of GHI values mentioned in the dataset.Since we run the experiment for arbitrary airspace, we randomly choose each sector's GHI values from the range of values, thereby preserving the realistic nature of GHI values.

C. Experimental Results

The flight paths obtained from applying Dijkstra's Algorithm on the airspace graph $\mathcal{G}^{\mathcal{A}}$ give the shortest paths solely in terms of edge cost or distance traveled by the aircraft. The S-POSCA algorithm provides a path that maximizes the solar cover while ensuring that the aerial vehicle does not stray away from approaching the destination, owing to the phototropic index used in the system model. On running the algorithm for different sets of origin and destination sectors (referred to as routes) for randomly chosen values of $G(s_i)$, $\mathcal{C}(s_i)$ and $\mathcal{P}(s_i)$, we observe an increase in the mean cumulative GHI of the flight path for S-POSCA as compared to regular Dijkstra,

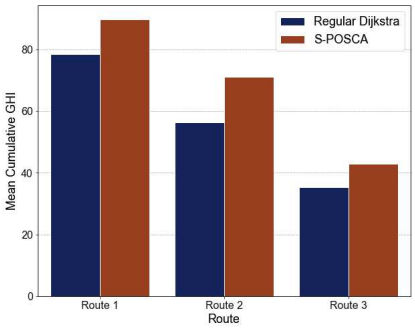

Fig. 7. Mean Cumulative GHI (without traffic).

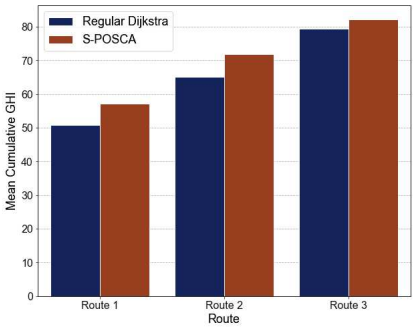

Fig. 8. Mean Cumulative GHI (with traffic).

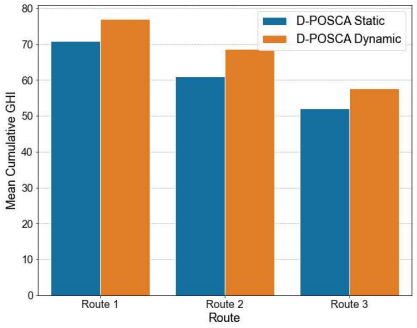

Fig. 9. Mean Cumulative GHI for Static and Dynamic Implementation of D-POSCA.

thus translating to increased solar charging of the aerial vehicle when used in real applications.

For analysis, 10 different iterations with different $G(s_i)$ values were run for each flight route. The mean cumulative GHI values obtained for regular Dijkstra and S-POSCA for each route without considering traffic congestion are shown in Fig. 7, where S-POSCA achieves an average increase of 20.58% in the mean cumulative GHI over all the routes. While considering traffic congestion, the same was repeated where in each iteration the $\mathcal{C}(s_i)$ and $\mathcal{P}(s_i)$ were different, chosen at random (Fig. 8). In this case, the average increase in the mean cumulative GHI was observed to be 8.81%, thus signifying considerable improvement in solar cover in both cases.

The D-POSCA algorithm was employed for application in a dynamic scenario, where the $G(s_i)$ values of the sectors can change while the vehicle is in transit. When the vehicle starts its trip, the algorithm initially provides a path from s_o to s_d. On running 300 iterations, we observed that this was the same path suggested by S-POSCA to be used in the static condition. However, for examining the efficiency and viability of using the D-POSCA algorithm to account for the dynamic nature of GHI in the sectors, the path is recalculated after each transition the vehicle makes from one sector to the next, as per the path output in the previous step. Thus, the final path that the vehicle undertakes is the result of recalculating the path from each sector to the destination s_d, which might be different from the path initially suggested by the same algorithm at the beginning of the trip. Fig. 9 compares the results of these two outputs, indicating improvement of the dynamic condition over the static one, exhibiting an average increase in the mean cumulative GHI by 10.64%. The distribution of the cumulative GHI values for various routes is shown in Fig. 10.

VI. Case Study of ALIA-250

To illustrate the significant gain in electrical power achievable by our proposed method, we consider a commercially available solar cell, the Maxeon™ C60, which has an area of $153cm^2$ and is at least 23% efficient [25]. Considering application in a commercial eVTOL aircraft such as the ALIA-250, which has a wingspan of $50ft$ [26], we assume an average chord length of $4ft$, which is pretty standard in the aerospace industry (as its actual value is not publicly

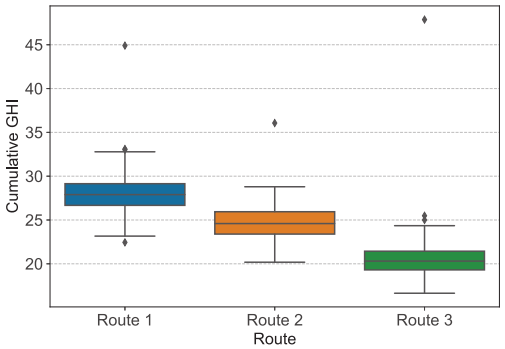

Fig. 10. Cumulative GHI Distribution for different Routes.

available), thereby having a wing area of $200ft^2$, or $18.58.m^2$. Thus, approximately 1214 C60 solar cells can be combined to form a solar panel mounted on the wing. Considering an example of a cumulative GHI of $100W/m^2$ obtained without using POSCA, we consider the increase of 10.64% in the GHI amounting to $110.64W/m^2$. In such a scenario, the ALIA-250, with the solar panel configuration mentioned earlier, will have $10.64W/m^2 \times 0.0153m^2 \times 0.23 \times 1214 = 45.45W$ of extra electrical power available as a result of using POSCA. Even though it might not seem too significant, it is to be noted that this is just for one UAM vehicle for one trip. Considering a very initial level implementation of UAM where a vehicle completes 10 trips per day, and there are 20 such vehicles in operation, it translates to $45.45 \times 10 \times 20 = 9090W$ or around 9KW of electrical power harnessed from solar energy daily.

VII. Features and Limitations of POSCA

POSCA exhibits two important features. Namely, it provides a path to maximize solar charging while meeting the travel time constraint, ensuring that the increase in travel time by straying from the shortest path solely in terms of distance is bounded and does not adversely affect the user's travel time experience. Furthermore, POSCA is not restricted to operating only in areas with adequate solar cover. In areas with no or insignificant solar cover (like nighttime), the Phototropic Index's contribution to the airspace graph's edge weights will be similar for all sectors. Hence, POSCA reduces to regular Dijkstra, constrained by only the sector capacities.

The limitations of POSCA are listed below.

- The aircraft movement is assumed to be from center to center of each sector, which is restrictive. Thus, POSCA can be augmented with advanced path-planning algorithms that consider more flexible trajectories.
- Relevant traffic flow models tailored to UAM can be incorporated into POSCA to accurately model the movement of other aircraft in the shared airspace.
- The model's scalability can be tested over a larger airspace while incorporating parameters such as wind speed and direction. Additionally, POSCA can be tested over a real-world test bed for prototyping, paving the way for commercialization in the future.
- POSCA can be extended to incorporate vertical transitions, offering exciting possibilities for three-dimensional (3D) path-planning algorithms utilizing multiple levels of airspace for UAM. Mobile agent-based communications [27] for the 3D airspace can also be explored.

VIII. Conclusion

This paper introduces POSCA, a novel Phototropic Index-driven path planning framework, addressing two problem variants, static and dynamic, using S-POSCA and D-POSCA. While Dijkstra's algorithm inspires S-POSCA, D-POSCA capitalizes on the efficiency of D* Lite to dynamically re-plan flight paths after each sector traversal, adapting to varying sunlight conditions. Simulation results reveal an 8.81% increase in total GHI encountered by the UAM vehicle in static weather conditions and a 10.64% increase in dynamic conditions. The significance of this improvement is exemplified in the case study undertaken wherein a 10.64% increase translates to harnessing about $9KW$ of electrical power from solar energy daily. This shows the viability of large-scale use of this scheme to increase UAM's sustainability quotient.

Acknowledgements: This work was supported by NSF grants OAC-2104078, SaTC-2030624, and ECCS-2319995.

References

[1] J. Pons-Prats, T. Živojinović, and J. Kuljanin, "On the understanding of the current status of urban air mobility development and its future prospects: Commuting in a flying vehicle as a new paradigm," *Transportation Research Part E: Logistics and Transportation Review*, vol. 166, p. 102868, 2022.

[2] "TomTom Traffic Index," 2023. Online: https://www.tomtom.com/traffic-index/.

[3] C. Alcock, "Beta and Blade Air Mobility Demonstrate ALIA-250 eVTOL Aircraft In New York Area," 2023. Online: https://futureflight.aero/news-article/2023-02-14/beta-and-blade-air-mobility-demonstrate-alia-250-evtol-aircraft-new-york.

[4] CNBC and News, "Spacex-backed startup says preorders for its $300,000 futuristic flying car have reached 2,850," 2024. Online: https://www.cnbc.com/2024/03/04/flying-car-firm-alef-hits-2850-preorders-worth-over-850-million.html.

[5] "Fortune Business Insights: Report #106344," 2021. Online: https://www.fortunebusinessinsights.com/urban-air-mobility-uam-market-106344.

[6] M. Tojal and L. Paletti, "Is urban air mobility environmentally feasible? defining the guidelines for a sustainable implementation of its ecosystem," *Transportation Research Procedia*, vol. 72, pp. 1747–1754, 2023.

[7] P. Zhao, J. Post, Z. Wu, W. Du, and Y. Zhang, "Environmental impact analysis of on-demand urban air mobility: A case study of the Tampa Bay Area," *Transportation Research Part D: Transport and Environment*, vol. 110, p. 103438, 2022.

[8] A. Liberacki, B. Trincone, G. Duca, L. Aldieri, C. P. Vinci, and F. Carlucci, "The Environmental Life Cycle Costs (ELCC) of Urban Air Mobility (UAM) as an input for sustainable urban mobility," *Journal of Cleaner Production*, vol. 389, p. 136009, 2023.

[9] W. Qu, C. Xu, X. Tan, A. Tang, H. He, and X. Liao, "Preliminary Concept of Urban Air Mobility Traffic Rules," *Drones*, vol. 7, p. 54, 01 2023.

[10] M. Rimjha, M. Li, N. HInze, S. Tarafdar, S. Hotle, H. Swingle, and A. Trani, "Demand Forecast Model Development and Scenarios Generation for Urban Air Mobility Concepts," 2020.

[11] S. Erb, M. Kobitzsch, and P. Sanders, "Parallel bi-objective shortest paths using weight-balanced b-trees with bulk updates," in *Experimental Algorithms* (J. Gudmundsson and J. Katajainen, eds.), (Cham), pp. 111–122, Springer International Publishing, 2014.

[12] D. Sengupta and S. K. Das, "Urban Air Mobility: Vision, Challenges and Opportunities," in *2023 IEEE 24th International Conference on High Performance Switching and Routing (HPSR)*, pp. 1–6, 2023.

[13] S. J. Carlson, T. Karakurt, P. Arora, and C. Papachristos, "Integrated solar power harvesting and hibernation for a recurrent-mission vtol micro aerial vehicle," in *2022 International Conference on Unmanned Aircraft Systems (ICUAS)*, pp. 237–244, 2022.

[14] S. J. Carlson, B. Moore, T. Karakurt, P. Arora, T. Cooper, and C. Papachristos, "The Gannet Solar–VTOL: An Amphibious Migratory UAV for Long–Term Autonomous Missions," in *2023 International Conference on Unmanned Aircraft Systems (ICUAS)*, pp. 419–424, 2023.

[15] O. Montagnier and L. Bovet, "Optimisation of a solar-powered high altitude long endurance UAV," in *Proceedings of the 27th International Congress of the Aeronautical Sciences*, 2010.

[16] A. Brown and W. L. Harris, "Vehicle Design and Optimization Model for Urban Air Mobility," *Journal of Aircraft*, vol. 57, no. 6, pp. 1003–1013, 2020.

[17] V. S. Dwivedi, Salahudden, D. K. Giri, A. K. Ghosh, and G. M. Kamath, "Optimal Energy Utilization for a Solar-Powered Aircraft Using Sliding-Mode-Based Attitude Control," *IEEE Transactions on Aerospace and Electronic Systems*, vol. 57, no. 1, pp. 105–118, 2021.

[18] S. Vaidhun, Z. Guo, J. Bian, H. Xiong, and S. K. Das, "Dynamic Path Planning for Unmanned Aerial Vehicles Under Deadline and Sector Capacity Constraints," *IEEE Transactions on Emerging Topics in Computational Intelligence*, vol. 6, no. 4, pp. 839–851, 2022.

[19] G. Li, A. Yamashita, H. Asama, and Y. Tamura, "An efficient improved artificial potential field based regression search method for robot path planning," in *2012 IEEE International Conference on Mechatronics and Automation, ICMA 2012*, pp. 1227–1232, 2012.

[20] S. Koenig and M. Likhachev, "D*lite.," in *Proceedings of the National Conference on Artificial Intelligence*, pp. 476–483, 01 2002.

[21] C. Chin, V. Qin, K. Gopalakrishnan, and H. Balakrishnan, "Traffic management protocols for advanced air mobility," *Frontiers in Aerospace Engineering*, vol. 2, p. 1176969, 2023.

[22] E. W. Dijkstra, "A note on two problems in connexion with graphs," *Numerische mathematik*, vol. 1, no. 1, pp. 269–271, 1959.

[23] NSRDB Dataset, "Solar Resource Data, Tools, and Maps," 2023. Online: https://www.nrel.gov/gis/solar.html/cite.

[24] M. Sengupta, Y. Xie, A. Lopez, A. Habte, G. Maclaurin, and J. Shelby, "The National Solar Radiation Data Base (NSRDB)," *Renewable and Sustainable Energy Reviews*, vol. 89, pp. 51–60, 2018.

[25] S. J. Carlson and C. Papachristos, "Solar Energy Harvesting for a Land-to-Recharge Tiltrotor Micro Aerial Vehicle," in *2022 IEEE Aerospace Conference (AERO)*, pp. 1–8, 2022.

[26] The Vertical Flight Society, "Beta Technologies ALIA 250," 2024. Online: https://evtol.news/beta-technologies-alia/.

[27] J. Cao, X. Feng, J. Lu, and S. K. Das, "Mailbox-based scheme for mobile agent communications," *Computer*, vol. 35, no. 9, pp. 54–60, 2002.